Ceramics International 47 (2021) 7593–7601

Contents lists available at ScienceDirect

Ceramics International

journal homepage: www.elsevier.com/locate/ceramint

Electrochemical performance of polymer-derived SiOC and SiTiOC ceramic electrodes for artificial cardiac pacemaker applications

Jongmoon Jang [a,*,1], Pradeep Vallachira Warriam Sasikumar [b], Fatemeh Navaee [c], Lorenz Hagelüken [a], Gurdial Blugan [b], Juergen Brugger [a,**]

[a] Microsystems Laboratory (LMIS1), École Polytechnique Fédérale de Lausanne (EPFL), 1015, Lausanne, Switzerland
[b] Laboratory for High Performance Ceramics, Swiss Federal Laboratories for Material Science and Technology (Empa), 8600, Duebendorf, Switzerland
[c] Microsystems Laboratory (LMIS4), École Polytechnique Fédérale de Lausanne (EPFL), 1015, Lausanne, Switzerland

ARTICLE INFO

Keywords:
Polymer-derived ceramic
Stimulation electrode
Electrochemical characterization
Pacemaker electrode

ABSTRACT

In an implantable electrode, such as a pacemaker electrode, fibrotic tissue formation due to a foreign body reaction is an important challenge affecting the efficiency to transmit the electrical signal of the device. The chemical inertness, biocompatibility, and electrical conductivity of polymer-derived ceramics (PDCs) are promising features in terms of overcoming this challenge. Here, the electrochemical behavior of polymer-derived silicon oxycarbide (SiOC) and titanium-doped SiOC (SiTiOC) ceramic electrodes for use as pacemaker electrodes is investigated by measuring impedance spectroscopy and cyclic voltammetry. In addition, typical stimulation electrodes such as iridium oxide, titanium nitride, platinum, and glassy carbon were prepared and loaded simultaneously into a custom-made electrochemical testing platform for comparison with SiOC and SiTiOC electrodes under identical conditions. The SiOC and SiTiOC electrodes shows a wide electrochemical stability window in the range of −0.9 to 1.2 V with a double layer capacitance as the charge injection mechanism at the electrode/phosphate-buffered saline interface. Also, analyzing the voltage transient shows that the maximum charge injection of the SiTiOC electrode was about 28 μC/cm^2. The results of the electrochemical evaluation and comparison of SiOC and SiTiOC stimulating electrodes will be helpful to understand fundamental characteristics for the potential of this material as candidate for next-generation pacemaker electrodes.

1. Introduction

An artificial cardiac pacemaker is an implantable medical device that senses heart beating rate and stimulates the heart muscles to pump blood [1]. The electrode at the end of the lead in the pacemaker is an essential component for delivering electrical stimulation to the cardiac muscle chamber [2]. State-of-the-art metal electrodes for pacemakers cause inflammation or fibrotic tissue, which in turn increases the impedance of the electrode, lowers overall electrical efficiency, and reduces battery life span [3–5]. Various studies to overcome these challenges include the development of a novel electrode geometry to minimize foreign body reaction [6,7], functional surface treatment [8], steroids eluted simultaneously with electrode insertion [9,10], and application of new emerging materials such as carbon nanotubes and poly (3,4-ethylenedioxythiophene):poly (styrenesulfonate) [11,12].

Ceramics have been applied as implantable prostheses on the basis of their biocompatibility, chemical inertness, mechanical hardness, and wear resistance [13–15]. Currently, the implantable ceramic prosthesis includes dental [16,17] and bone implants [13,18], electronic packaging [15] as well as scaffolds for tissue regeneration [19,20]. In particular, polymer-derived ceramics (PDCs) [21], which are obtained by the pyrolysis of preceramic polymer precursors under an inert atmosphere, are advantageous due to their tunable material properties, structural 3D shaping [22–26] for implantable electrode application, and lower temperature required for polymer-to-ceramic conversion [27–31]. In our previous works, electrical properties of carbon-rich conductive silicon oxycarbide (SiOC) PDC electrodes were investigated [32,33], and their passive (unstimulated) cytotoxicity was evaluated for pacemaker electrode application [34]. Recently, cytocompatibility of a titanium-doped SiOC (SiTiOC) PDC electrode with 20 wt% Ti content

* Corresponding author.
** Corresponding author.
E-mail addresses: jongmoon@kims.re.kr (J. Jang), juergen.brugger@epfl.ch (J. Brugger).
[1] Present address: Korea Institute of Materials Science (KIMS), 51508 Changwon, Republic of Korea.

https://doi.org/10.1016/j.ceramint.2020.11.098
Received 15 October 2020; Received in revised form 11 November 2020; Accepted 15 November 2020
Available online 19 November 2020

was confirmed by monitoring cells under pacing (active stimulation) conditions [35].

In addition to the conductivity and cytotoxicity of a material for implantable PDC electrodes, it is also essential to understand the electrochemical characteristics at the electrode/electrolyte and electrolyte/tissue interface since the charge injection mechanism, impedance, and potential limits are material dependent [36,37]. Norlin et al. investigated the electrochemical behavior of the state-of-the-art pacemaker electrodes such as platinum (Pt), titanium (Ti), and titanium nitride (TiN) [38–41]. Weigel et al. developed a 3D carbon fiber with a 2D TiN electrode to assess the inflammatory response at the cardiac tissue-electrode interface [6]. Grossenbacher et al. estimated the electrochemical properties of a microelectromechanical system (MEMS)-based glassy carbon (GC) for a pacemaker electrode [42]. Various materials also have been studied for implantable electrode applications such as neurological disorder, cochlear implant, and artificial retina [43–49]. However, to date, studies have been rarely conducted that are systematically investigating the electrochemical properties of the PDC electrodes as a stimulating electrode for pacemaker applications, especially comparing them thoroughly with various types of metal and GC electrodes.

In addition, for electrochemical investigation, a testing platform is essential to stably assess the electrode properties or to perform *in vitro* experiments by considering the varying geometric surface area and the wiring issues of the electrodes. Hou et al. have successfully developed a testing platform to investigate the electrochemical properties of a multi-electrode array [50]. A multifunctional testing platform reported by Zhang et al. was used to perform electrochemical studies with cell culture for drug screening [51]. However, a highly integrated platform capable of reliably analyzing electrochemical properties while maintaining consistent geometric surface area of different types of electrodes with various dimensions and even *in vitro* cell analysis has not been exploited so far.

In this paper, polymer-derived SiOC and SiTiOC ceramic electrodes and representative stimulation electrodes such as iridium oxide (IrO_2), Pt, TiN, and GC were fabricated and integrated with a custom-made testing platform to characterize their electrochemical properties for pacemaker application. The electrochemical behavior of SiOC and SiTiOC electrodes at the electrode/phosphate-buffered saline interface was assessed by electrochemical impedance spectroscopy (EIS) and cyclic voltammetry (CV), and the results were compared with those of other fabricated stimulation electrodes. In addition, electrical current stimulation was applied to a SiTiOC electrode at the interface to analyze the voltage transient to estimate the maximum charge injection. Furthermore, cytotoxicity of the SiTiOC electrode-integrated testing platform was evaluated by culturing cardiac cells.

2. Experimental

2.1. Fabrication of the stimulation electrodes

A 100-mm-diameter glass wafer (thickness: 525 μm) was cut into 6 × 6 mm^2 size by a dicing saw (DAD321, DISCO Corp., Japan) as the electrode substrate and Pt, IrO_2, and TiN (50 nm thick for each of them) were deposited by sputtering (DP 650, Alliance Concept, France). The front and back sides of the substrate, including the sidewalls, were coated with above-mentioned metals for the wiring with the electrical pad on the printed circuit board (PCB).

A 1-μm-thick SiO_2 layer was wet-oxidized on the surface of a silicon wafer as a sacrificial layer. SU-8 (GM 1075, Gersteltec, Switzerland) was spin-coated on the sacrificial layer and patterned using a negative photolithography process. A 200 μm-thick SU-8 discs structure having a diameter of 10 mm was then released by wet etching using a buffered oxide etchant (NH_4F 40% + HF 50%, 7:1) for two days. The freestanding SU-8 structures were cleaned and pyrolyzed in a tube furnace (PEO 601, ATV Technologies GmbH, Germany) under a constant nitrogen gas flow of 2000 mL/min. Another SiO_2 coated silicon wafer was placed on top as a weight to avoid structural deformation during heating/cooling. The furnace was first heated from room temperature to 200 °C at a rate of 10 °C/min and held at this temperature for 30 min, and then ramped to 900 °C at 10 °C/min and held at this maximum temperature for 1 h. The furnace was cooled to room temperature at a rate of 10 °C/min. Finally, a GC electrode with a diameter of 6 mm and a thickness of 100 μm was obtained. The vertical and horizontal shrinkage were 60 and 50%, respectively.

SiOC was synthesized by mixing polyhydromethyl siloxane (PHMS) and divinylbenzene (DVB) with Pt Karstedt's catalyst (Sigma-Aldrich, Switzerland). In a typical preparation, 2g of DVB was mixed with about 700 ppm of Pt catalyst by stirring for 15 min, and 1g of PHMS was added dropwise to the DVB mixture. After that, the mixture was stirred at room temperature for 30 min. The preceramic mixture was then casted in Polytetrafluoroethylene (PTFE) molds and left at room temperature. Gelation was observed within 30 min and the gels are left for overnight at ambient condition (*i.e.*, room temperature in a fume hood). Preceramic gels were then peeled off from the molds and cured at 80 °C for 48 h to complete cross-linking. The cured preceramic green bodies were then pyrolyzed in a tube furnace (Carbolite STF 16/450, Germany) under a constant argon flow. During pyrolysis, temperature was ramped up to 1000 °C at a rate of 50 °C/h and held for 1 h, and cooled to room temperature at 50 °C h. For the SiTiOC electrodes, 20 wt % titanium (IV) ethoxide (TiOET) is mixed with a PHMS/DVB mixture and the rest of the process was the same as the fabrication process of the SiOC electrodes. The detailed synthesis procedures of the amorphous SiOC and SiTiOC PDC electrodes and material characteristics were reported in our previous works [32,35].

2.2. Manufacturing of the testing platform

A master mold was manufactured using a 3D printer (FDM 400mc, Stratasys Inc., U.S.A) with ABS-M30 material to create the PDMS multi-wells. A 10 μm-thick parylene C (C30S, Comelec SA, Switzerland) was deposited on the surface of the fabricated mold to easily demold the PDMS multi-wells. The PDMS was filled in the fabricated mold at a rate of 1:10 wt ratio of curing agent and monomer and cured at 70 °C for 3 h. After demolding the PDMS structure, a 1 mm-diameter hole was punched on the center of each well to expose the surface of the stimulation electrodes. The electrodes and PDMS wells were bonded by a biocompatible glue (EPO-TEK 301, Epoxy Technology Inc., U.S.A) and a small drop of liquid metal (Ga–In, Sigma-Aldrich, Switzerland) was used to create electrical contact with low ohmic resistance to the back-side of the fabricated electrode and electrical pad of the PCB. All electrodes were wired independently for the individual characterization.

2.3. Electrochemical characterization

The electrochemical properties of all the fabricated electrodes loaded in the testing platform were characterized by measuring impedance spectroscopy, CV, and voltage transient. Phosphate-buffered saline (PBS; 1x, pH 7.4, Sigma-Aldrich, Switzerland) was used as an electrolyte considering an implantable electrode application, and an Ag/AgCl reference electrode (Skinny RE, Gamry Instruments, U.S.A) was immersed into the PBS as third electrode, as shown in Fig. 2 (d). A potentiostat (Reference 600+, Gamry Instruments, U.S.A) was used to measure the EIS and CV by maintaining a constant potential level of the working electrode with respect to the reference electrode.

2.4. Cardiac cell culturing on the PDC embedded platform

Primary rat neonatal cardiomyocytes were isolated by using a Pierce Primary Cardiomyocyte Isolation Kit, according to the manufacturer's instructions. The rat neonatal hearts were collected after birth and cut into pieces of about 1 mm thickness. The pieces were washed with Hanks

Balanced Salt Solution (HBSS) to remove blood cells and incubated with Pierce Cardiomyocyte Isolation Enzyme 1 and 2 for 35 min. Another washing step was performed and the heart tissue was disrupted in Complete DMEM for Primary Cell Isolation by pipetting up and down 25 to 30 times. Finally, single cells with a cell density of 10^6 cells/mL were seeded in the testing platform and placed in an incubator at 37 °C with 5% CO_2. Organ harvesting was performed on sacrificed control animals from unrelated experiments, according to license VD 3290 designed for this specific purpose. To evaluate cardiac cell viability after two days, the cultured cells were stained with a LIVE/DEAD Viability/Cytotoxicity Kit by Molecular Probes for 30 min. The green fluorescent, calcein-AM component, stains live cells and the red fluorescent, ethidium homodimer-1 component of the LIVE/DEAD kit, identifies the dead cells. A fluorescent microscope (Eclipse TE300, Nikon, U.S.A) was used to count live and dead cells and quantitative data were obtained using Image J software (US National Institutes of Health, U.S.A) by counting at four non-overlapping areas. To quantify the mechanical beating rate of the cells, movies were acquired by connecting a video camera to the microscope. Quantification of the beating frequency was performed by a Pulse software (Cellogy Inc., U.S.A).

3. Results and discussion

Six types of stimulation electrodes were used in our studies consisting of metal (Pt, IrO_2, and TiN), SU-8 derived GC, and PDC electrodes (SiOC and SiTiOC), as shown in Fig. 1a. The fabrication process for the all metal electrodes (i), GC (ii), and PDC electrodes (iii) is shown in Fig. 1b. The fabricated stimulation electrodes were integrated into our testing platform to investigate the electrochemical behavior, as shown in Fig. 2a. The testing platform was assembled with a PCB, the fabricated electrodes, and PDMS multi-well plates, as shown in the exploded view of Fig. 2b. The platform consists of 4 by 4 PDMS multi-wells and each single well has two channels to load the working electrodes (WE) such as IrO_2 (n = 3), TiN (n = 3), Pt (n = 2), glassy carbon (n = 2), SiOC (n = 3), and SiTiOC (n = 3) on the right side and Pt as counter electrodes (CE) on the left side. The fabricated electrodes were exposed at the bottom of each PDMS well through the punched 3 mm-diameter cut-out resulting in a geometric surface area (GSA) of all electrodes of 0.706 cm^2. Between each well a narrow channel was defined to connect both wells by the electrolyte. Fig. 2c shows an optical image of the fabricated testing platform.

Phosphate-buffered saline (PBS; 1x, pH 7.4) was used as the electrolyte, and the Ag/AgCl reference electrode (RE) was immersed into PBS for a three-electrode cell method, as shown in Fig. 2 (d). EIS was measured to evaluate the electrochemical behavior of the fabricated stimulation electrodes. To avoid overlapping plots, the results were assorted into two categories as metal electrodes and GC/PDC electrodes. Fig. 3a and b shows Bode plots of magnitude and phase versus frequency for representative EIS spectra of metal electrodes in the range of 1 Hz–100 kHz. The magnitude of impedance decreased as the frequency increased with a phase shift from 0 to −90°. We analyzed the low-frequency (10 Hz) impedance considering the electromyography and pacing, and the high-frequency (1 kHz) impedance for general neural recording/stimulation, respectively [38]. The impedance of IrO_2 was the lowest at 8.7 ± 1.1 kΩ at 10 Hz, and the impedance of Pt was the lowest at 350 ± 18 Ω at 1 kHz. Fig. 3c and d shows the magnitude and phase for the GC, SiOC, and SiTiOC electrodes. The impedance of both PDC electrodes at 10 Hz was relatively higher than that of the metal and GC electrodes, respectively, while the impedance of the SiTiOC electrode at 1 kHz was at a similar level with that of the IrO_2 electrode. The detailed impedance of each electrode at 10 Hz and 1 kHz is shown in Table 1. In addition, these EIS results were fit to an equivalent electrical circuit model by analysis software (Echem Analyst, Gamry Instruments, U.S.A), as shown in the inset of Fig. 3c. The elements of the equivalent circuit

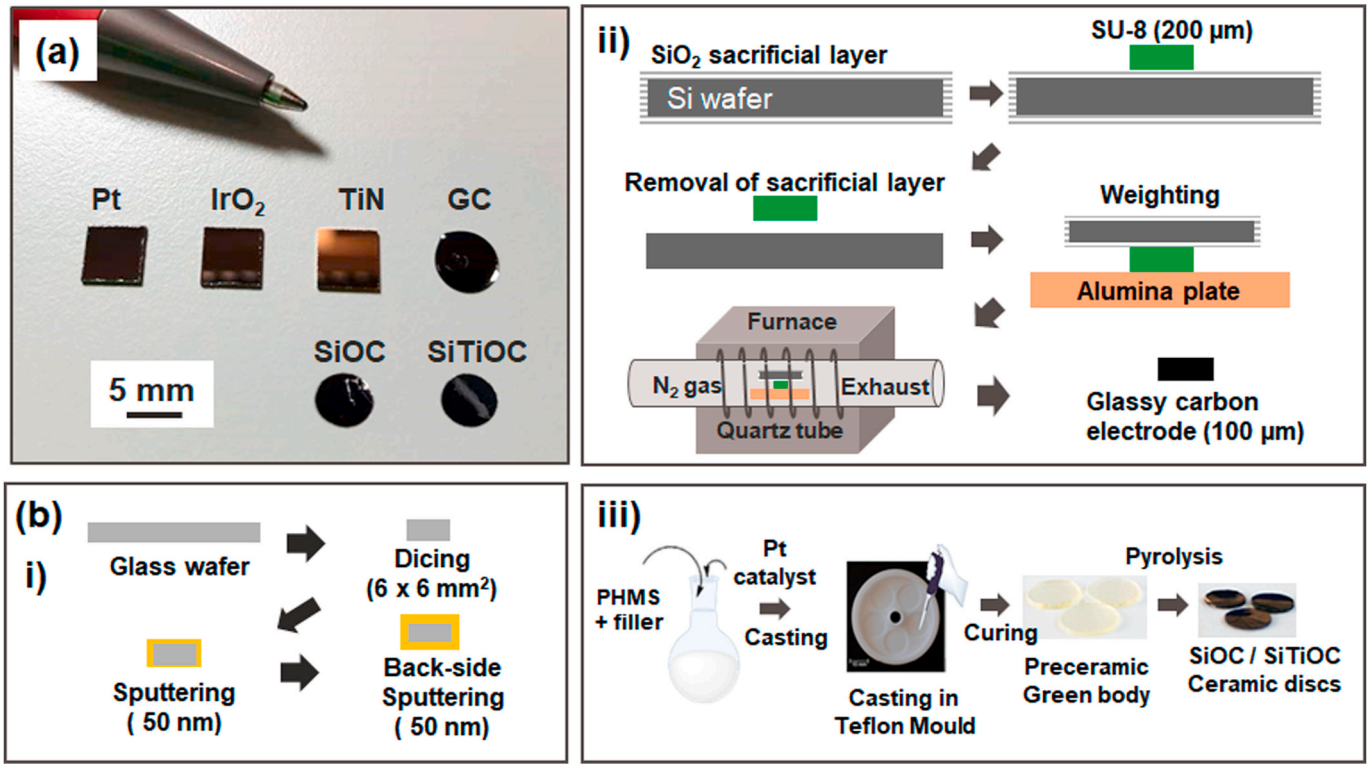

Fig. 1. (a) Optical image of the fabricated platinum (Pt), iridium oxide (IrO_2), titanium nitride (TiN), glassy carbon (GC), polymer-derived silicon oxycarbide (SiOC) ceramic, and titanium-modified silicon oxycarbide (SiTiOC) ceramic electrodes. (b) Schematic drawing of the fabrication process for the (i) Pt, IrO_2, TiN electrode (ii) GC electrode, and (iii) polymer-derived SiOC and SiTiOC ceramic electrodes [20]. (For interpretation of the references to colour in this figure legend, the reader is referred to the Web version of this article.)

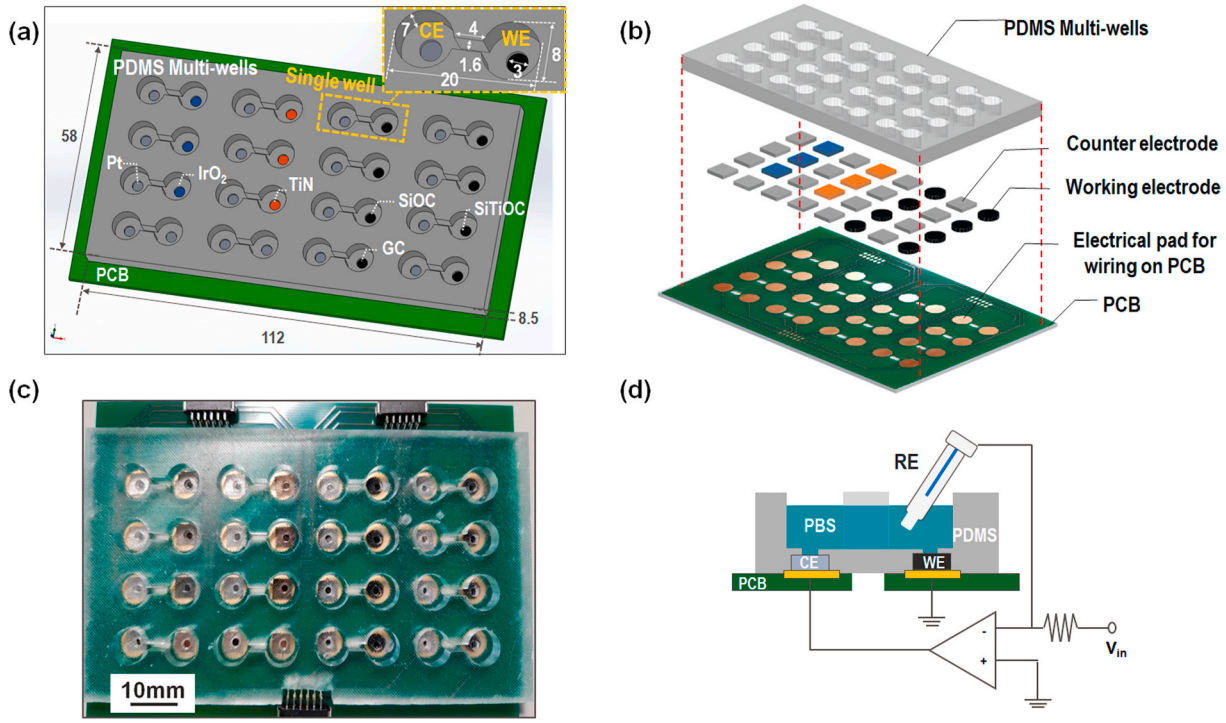

Fig. 2. (a) Schematics for the electrochemical testing platform to characterize polymer-derived ceramic electrodes with various stimulation electrodes. The inset is an enlarged single well embedded with a working electrode (WE) and a counter electrode (CE) (b) Exploded view for manufacture of the platform, which consists of a printed circuit board (PCB) for electrical connection, polydimethylsiloxane (PDMS) based multi-wells to contain electrolytes, and stimulation electrodes, (c) Optical image of the manufactured electrochemical testing platform with various stimulation electrodes. (d) Schematic drawing showing the three electrode method to investigate electrochemical behaviors of the stimulation electrodes (RE: reference electrode).

modeling are as follows: the polarization resistance (R_p), electrolyte solution resistance (R_u), constant phase element (CPE), and Warburg impedance for diffusion (W_d). CPE is used to investigate the double layer effect at the electrode/electrolyte interface as the double layer capacitance is not a perfect capacitor. The admittance of CPE (Y_{CPE}) can be described using the following equation [52].

$$Y_{CPE} = Y_0(j\omega)^{\alpha} \quad (1)$$

where ω denotes the angular frequency (rad/s) and α is a parameter to fit a constant phase (*i.e.*, frequency independent) and ranges from 0 to 1 (CPE represents the ideal capacitor if $\alpha = 1$), and Y_0 denotes double layer capacitance of the stimulation electrodes. The primary mechanism for transferring charge at the electrode/electrolyte interface is double layer capacitance and faradaic reaction [36]. Double layer capacitance includes redistribution of charged chemical species in the electrolyte without transferring the electron, while the faradaic reaction is induced by a reduction or oxidation with transfer of electrons. Y_0 of the TiN and GC electrode ($3.2e^{-7}$ and $2.5e^{-7}$ $S{\cdot}s^{\alpha}$) was significantly higher than that of IrO_2 and Pt ($5.9e^{-9}$ and $8.3e^{-9}$ $S{\cdot}s^{\alpha}$), which is consistent with the charge injection mechanism of TiN and GC is 'capacitive' while the mechanism of IrO_2 and Pt is a 'faradaic' reaction at the interface. Y_0 values of SiOC and SiTiOC PDC electrodes ($1.8e^{-7}$ and $3.3e^{-7}$ $S{\cdot}s^{\alpha}$) were larger than those IrO_2 and Pt, and are at a similar level with those of TiN and GC electrodes. Therefore, the double layer capacitance is dominant in the charge injection mechanism of the SiOC and SiTiOC PDC electrodes. In addition, the faradaic impedance (Z_F) was derived as follows [53]:

$$Z_F = R_P + W_d/(jw)^{1/2} \quad (2)$$

The Z_F of the GC and PDC electrodes was relatively higher than that of other electrodes, identifying the capacitive charge injection as the dominant charge injection mechanism. The fit parameters of all stimulation electrodes were described in Table 2.

Fig. 4a shows the CV curves of IrO_2, TiN, and Pt at a sweep rate of 25 mV/s. The IrO_2 electrode shows distinct oxidation and reduction peaks at 0.25 (peak number: 1) and 0.2 V (peak number: 2), and the reduction peak of Pt was observed at around −0.4 V (peak number 3). The results are consistent with the charge injection mechanism of IrO_2 and Pt being faradaic reaction. Fig. 4b shows an enlarged CV curve of the TiN electrode in (a), which differs from the CV of IrO_2 and Pt electrodes. Redox peaks were not observed in the range of −0.9 to 1 V, which confirms that the charge injection mechanism of the TiN electrode is capacitive. Also, as shown in Fig. 4c, no redox peaks were obtained in the CV curve of the GC electrode, confirming the capacitive charge injection mechanism. Magnified CV curves of the SiOC and SiTiOC PDC electrodes are shown in Fig. 4d. Larger potential limits were applied to identify the electrochemical stability window without having any redox reaction. For the SiOC electrode, the reduction peak (peak number 1) was observed at −1 V, and SiTiOC electrode shows the oxidation peak (peak number 2) at around −1 V. Therefore, the water window of SiOC and SiTiOC was approximately in the range of −0.9 to 1.2 V. The charge injection mechanism of the PDC electrodes was capacitive in the water window. The electrochemical characteristics of each stimulation electrode obtained from EIS and CV are summarized in Table 1.

A previous study has already verified the cytocompatibility of SiTiOC electrodes under electrical stimulation, *i.e.*, pacing [35]. Here, the maximum charge that the SiTiOC electrode can inject at the electrode/electrolyte interface was investigated by analyzing the voltage transient. Fig. 5a shows the voltage signal measured at the RE by applying a charge-balanced biphasic stimulus current between the SiTiOC electrode and the Pt counter electrode. Fig. 5b shows an enlarged graph of the green dotted rectangle in (a) and the current applied at this time. The input current pulse was in the range of −20 – 20 μA with 1 ms pulse width of each positive/negative, and the rise/fall rate was 20 mV/s. The voltage transient response consists of the following parameters [37,54]: E_{ipp} (inter-pulse potential; *i.e.*, DC bias of the WE versus

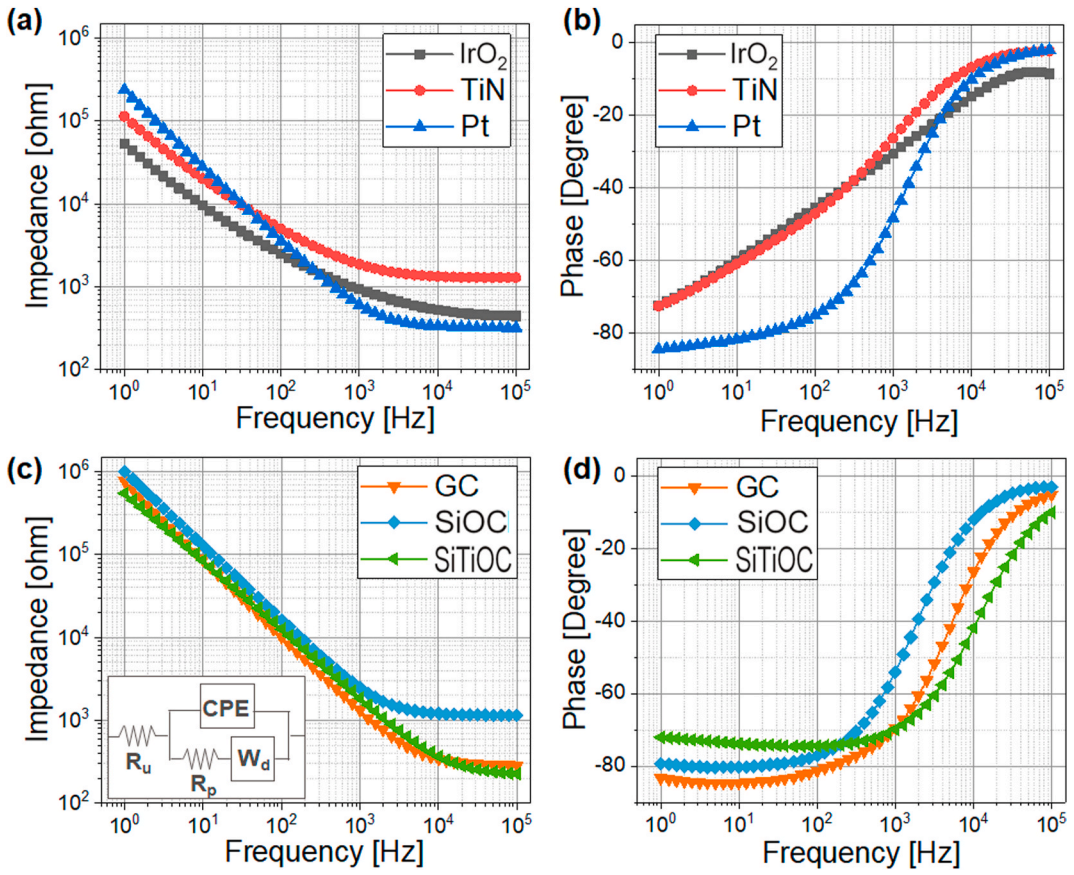

Fig. 3. (a) Magnitude and (b) phase of the representative electrochemical impedance spectroscopy (EIS) for the iridium oxide (IrO_2), titanium nitride (TiN), and platinum (Pt) electrode (c) magnitude and (d) phase of the representative EIS for the glassy carbon (GC) and polymer-derived SiOC and SiTiOC ceramic electrodes. The inset of (c) is an electrical equivalent circuit model to fit the EIS results.

Table 1
Magnitude of the impedance, charge injection mechanism, electrochemical potential stability window, and cathodal charge storage capacitance.

Stimulation electrode	IrO_2	TiN	Pt	SU-8 derived Glassy carbon	SiOC	SiTiOC
Impedance at 10 Hz [kΩ]	8.7 ± 1.1	18 ± 2.3	31 ± 4.8	71 ± 23	100 ± 25	99 ± 23
Impedance at 1 kHz [Ω]	490 ± 42	1100 ± 170	350 ± 18	310 ± 39	2200 ± 970	520 ± 140
Mechanism	Faradaic	Capacitive	Faradaic/Capacitive	Capacitive	Capacitive	Capacitive
Electrochemical stability window [V]	−0.6 – 0.8	−0.9 – 1	−0.6 – 0.8	−1 – 1	−0.9 – 1.2	−0.9 – 1.2
cCSC [μC/cm^2]	1200	50	170	1050	38	120

Table 2
The characteristic parameters of electrochemical impedance spectroscopy obtained by fitting the model in Fig. 3 (c).

Stimulation electrode	IrO_2	TiN	Pt	Glassy carbon	SiOC	SiTiOC
R_u [ohm]	430	1010	320	290	1100	210
Y_0 [S·s$^\alpha$]	5.9×10^{-9}	3.2×10^{-7}	8.3×10^{-9}	2.5×10^{-7}	1.8×10^{-7}	3.3×10^{-7}
α	0.75	0.71	0.90	0.93	0.90	0.85
W_d [S·s$^{1/2}$]	2.7×10^{-12}	2.1×10^{-13}	1.4×10^{-15}	1.1×10^{-14}	1.8×10^{-8}	1.2×10^{-6}
R_p [kohm]	15	327	17	68	21	250

RE), V_a (the access voltage associated with ohmic electrolyte resistance), E_{ma} (maximum positive polarization), and E_{mc} (maximum negative polarization). Both E_{ma} and E_{mc} are calculated by the following relationships:

$$E_{mc} = V_{max,\ neg} - V_a \quad (3)$$

$$E_{ma} = V_{max,\ pos} - V_a \quad (4)$$

where $V_{max,\ neg}$ and $V_{max,\ pos}$ are the maximum negative/positive voltage transient. As shown in Fig. 5b, the measured E_{ipp} was −0.71 V, V_a was 0.07 V, and the corresponding E_{ma} and E_{mc} were −0.65 and −0.87, respectively. Since E_{mc} almost reached the negative side of the electrochemical stability window of the SiTiOC electrode (*i.e.*, −0.9 V), the maximum charge injection (Q_{inj}) was obtained by multiplying the applied current with the pulse width, and by dividing the GSA of the electrode. Therefore, the Q_{inj} of SiTiOC calculated at the PBS interface was about 28 μC/cm^2, and does not damage the electrodes or tissues by the irreversible faradaic reaction at the interface until the corresponding

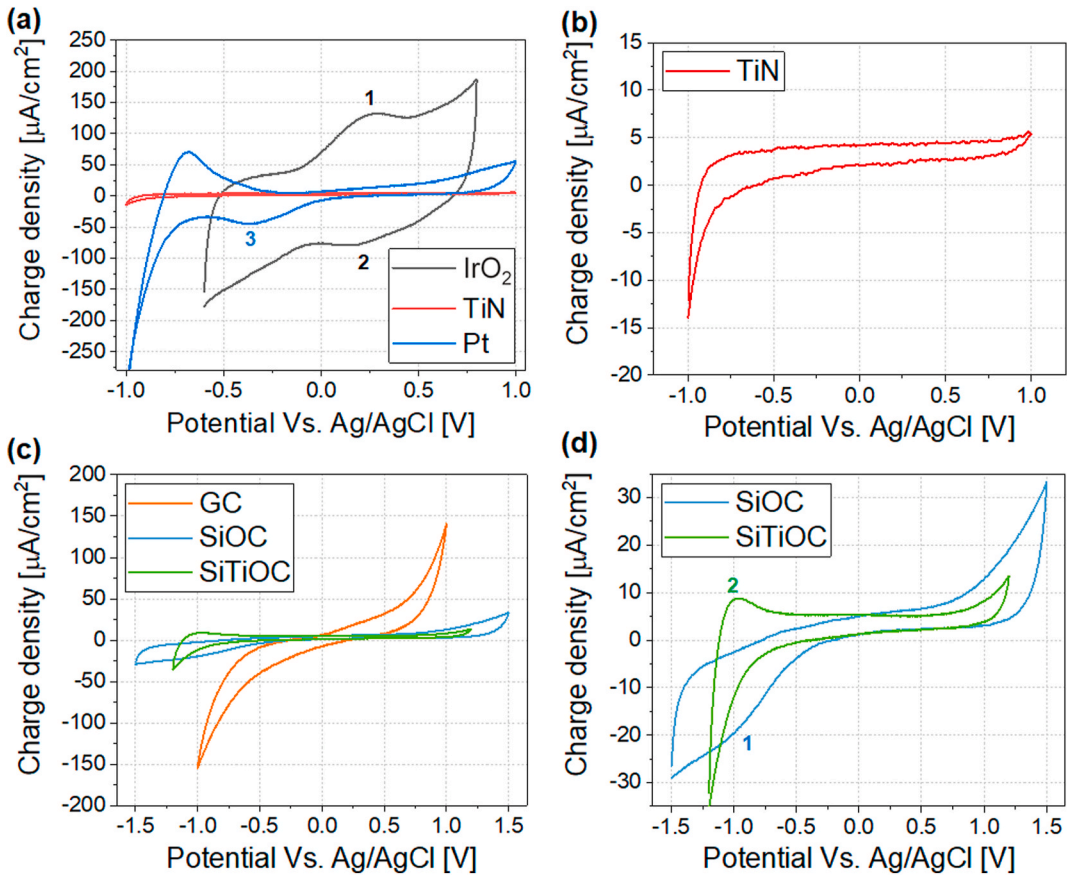

Fig. 4. (a) Cyclic voltammetry (CV) curve of the iridium oxide (IrO_2) electrodes; peaks number 1 and 2 are the redox reaction of IrO_2; peak number 3 is reduction of surface oxide. (b) Enlarged CV graph of the titanium nitride (TiN) from (a) (c) CV curve of the glassy carbon (GC), polymer-derived SiOC and SiTiOC ceramic electrodes (d) Enlarged CV graph of SiOC and SiTiOC electrodes; peak numbers 1 and 2 are the reduction and oxidation, respectively.

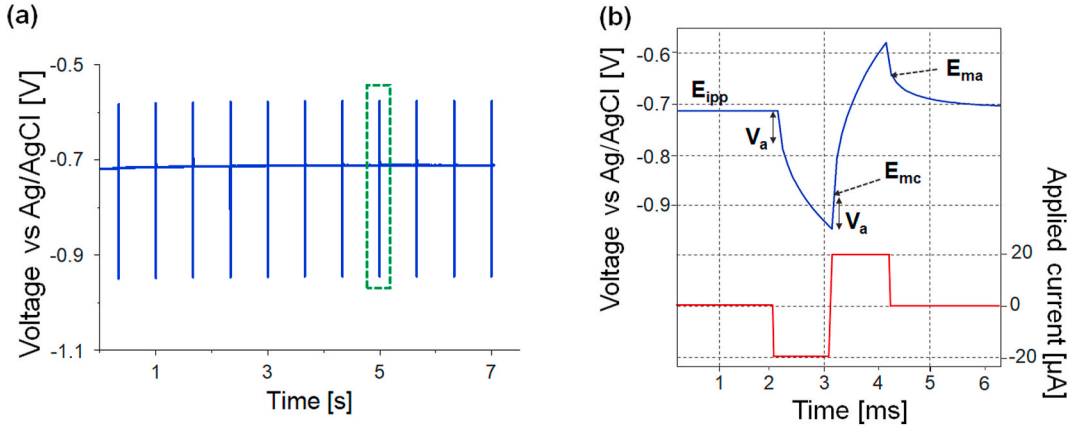

Fig. 5. (a) Voltage transient measurement applying to charge balanced biphasic stimulation current with short pulse width. The polymer-derived SiTiOC ceramic electrode was used as a working electrode and Ag/AgCl was used as a reference electrode (b) Enlarged graph of the green dotted rectangular inset of (a) to identify the voltage transient of the SiTiOC electrode. The applied current signal was plotted below the voltage waveform. (For interpretation of the references to colour in this figure legend, the reader is referred to the Web version of this article.)

charge injection.

To address the current challenges of pacemaker electrodes caused by fibrotic tissue in a foreign body reaction, the SiOC and SiTiOC PDC electrode have been investigated owing to its low creep rate, chemical inertness, and wear resistance. As a starting point for PDC to be used as an implantable electrode, the electrochemical properties were characterized and compared with those of other types of stimulation electrodes such as IrO_2, TiN, Pt, and GC. Although the SiOC and SiTiOC electrode has a higher impedance than the metal electrode at low frequency, it has a wide electrochemical stability window (−0.9 – 1.2 V) and double layer capacitance as the primary charge injection mechanism, which is similar with TiN and GC electrodes. However, the maximum Q_{inj} of SiTiOC is relatively low compared to that of other stimulation electrodes [37], but considering that no surface treatment was performed, it can be improved further by surface modification and functional coating as future work [55–58]. In addition, further investigation such as long-term impedance

evaluation, aging test, and evaluation of the corrosion characteristics should be performed to understand the possibilities of SiOC and SiTiOC PDCs for fabrication of pacemaker electrodes [47,59–61]. It is also important to understand immunological properties at the cardiac tissue/PDC electrode interface for practical applications [6]. In addition, state-of-the-art PDCs with various phase structures such as amorphous, glassy, and crystalline have been proposed with a variety of synthesis and processing methods [62–65]. Further assessment could be conducted in the near future to compare and analyze the electrochemical properties of these advanced PDC materials in view of a potential use as stimulating electrodes and explore their respective characteristics.

In order to assess the cytocompatibility, cardiomyocytes, which constitute the cardiac muscle and are involved in the contractile function for blood pumping [51,66], were cultured on a testing platform integrated with a SiTiOC PDC electrode. Primary cultured cardiomyocytes in the testing platform were stained with a LIVE/DEAD Viability/Cytotoxicity Kit to evaluate the cytotoxicity of the testing platform with SiTiOC electrodes. As shown in Fig. 6a, cultured cells in the PDMS channel between the two electrodes were analyzed using a fluorescent microscope. Fig. 6b (i-ii) shows the cell viability by representative fluorescent images with green and red, which were stained by calcein-AM and ethidium homodimer-1, respectively. As shown in Fig. 6b (iii), 90% of live cells were identified on the testing platform with the SiTiOC electrode, confirming biocompatibility of our testing system. Also, as shown in the supporting video V1, the beating behavior of cardiomyocytes were observed after five days of cell seeding, demonstrating a good cytocompatibility of SiTiOC with cardiomyocytes. In our previous studies, the cytotoxicity of SiOC and carbon-rich SiOC (50 wt % doped with the precursor) were evaluated using C2C12 myoblast cells for 24 h, which confirms the cytocompatibility of the SiOC PDCs [34]. Recently, the assessment of cell viability and metabolic activity was performed by cultivating normal human dermal fibroblasts (NHDF) with SiOC and SiTiOC for five days, confirming the cytocompatibility of SiOC with no harmful effect by Ti fillers [35]. These results are consistent with previous studies with Ca and Mg ions doped SiCaMgOC PDCs [67]. In the present study, the cytocompatibility of SiTiOC with cardiomyocytes was assessed for potential pacemaker applications. Further studies using cardiomyocytes at the cardiac tissue/PDC electrode interface are possible based on this testing platform, and subsequent *in vitro* studies such as cell beating modulation or electrocardiogram recording [51] could be performed in the near future.

Supplementary video related to this article can be found at https://doi.org/10.1016/j.ceramint.2020.11.098

4. Conclusion

In this paper, electrochemical behaviors of polymer-derived ceramic SiOC and SiTiOC electrodes were investigated for their application as

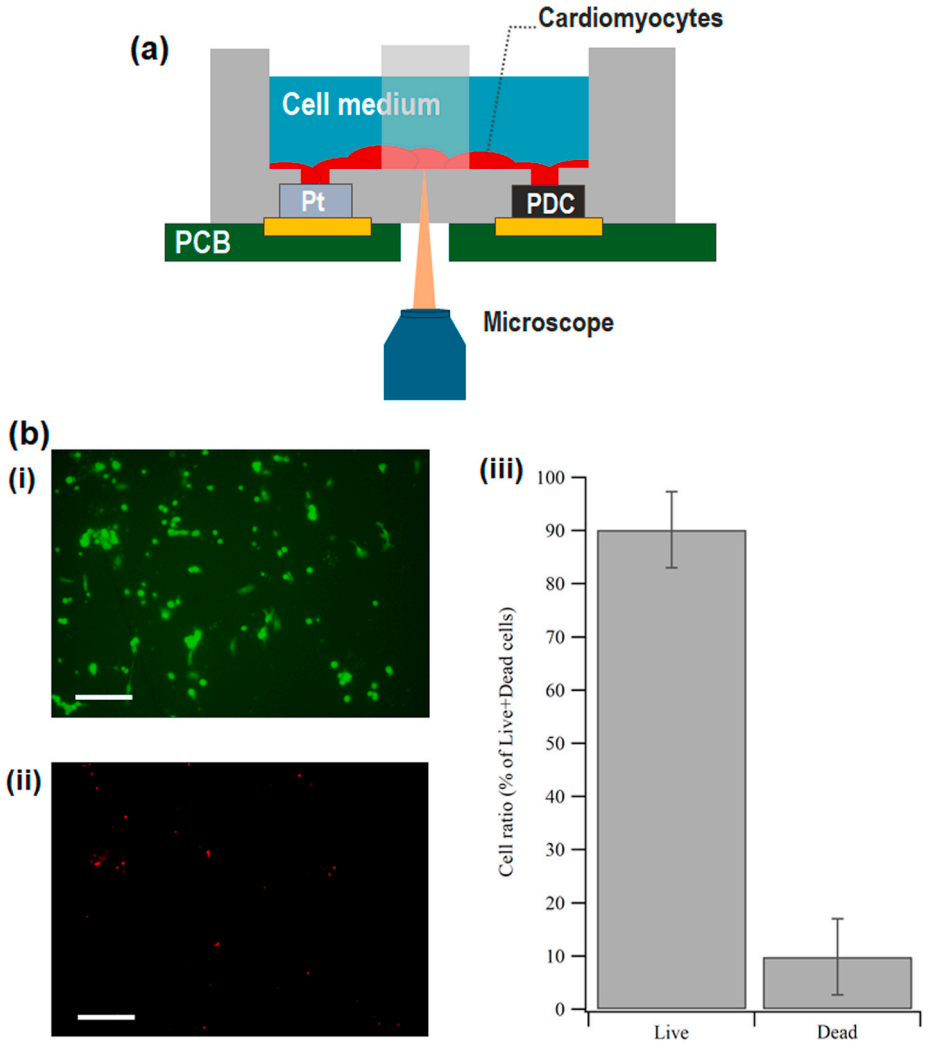

Fig. 6. (a) Schematic drawing of the cardiomyocytes seeding in the testing platform loaded with polymer-derived ceramic (PDC) electrode and platinum (Pt) electrode (b) Live/Dead cell viability assay coated slide at day 2: (i) optical fluorescent image of live (green) and (ii) dead (red) cells. Scale bar: 100 μm (iii) Viability of the cells ($n=4$). (For interpretation of the references to colour in this figure legend, the reader is referred to the Web version of this article.)

pacemaker electrodes and the properties were compared with those of typical stimulation electrodes such as IrO_2, Pt, TiN, and glassy carbon electrodes. The fabricated stimulation electrodes were integrated with a testing PDMS-multiwell platform to efficiently analyze the electrochemical characteristics of various stimulation electrodes simultaneously and under identical experimental conditions. The impedance of the SiOC and SiTiOC PDC electrodes was determined by measuring the EIS spectra, and its double layer capacitance was obtained by fitting the electrical equivalent circuit model. The impedance of the SiOC and SiTiOC electrodes was higher than that of Pt and IrO_2 electrodes, but similar to that of TiN and GC electrodes. In addition, a 'capacitive' charge injection mechanism was identified for the SiOC and SiTiOC electrodes with a relatively wide electrochemical stability window, similar to the cases of TiN and GC. Furthermore, the maximum charge injection of the SiTiOC PDC electrode was investigated by analyzing the voltage transient induced by applying biphasic stimulating current pulses. Finally, to demonstrate the applicability of various stimulation electrode-embedded platforms to conduct future studies for the tissue/electrode interface, cardiomyocytes were cultured on the testing platform with the PDC electrode and its biocompatibility was evaluated and confirmed.

Author contributions

The manuscript was written through contributions of all authors. All authors have given approval to the final version of the manuscript.

Declaration of competing interest

The authors declare that they have no known competing financial interests or personal relationships that could have appeared to influence the work reported in this paper.

Acknowledgments

The authors thank the Center of Micro/Nanotechnology (CMi) of EPFL for the microelectromechanical system (MEMS) fabrication support. This work is funded by an initiative of the ETH board through the Strategic Focus Area (SFA) – Advanced Manufacturing programme (project "Ceramic X.0 – High-precision micro-manufacturing of ceramics"), Switzerland.

References

[1] B. Lown, B.D. Kosowsky, Artificial cardiac pacemakers, N. Engl. J. Med. 283 (1970) 907–916.
[2] K. Stokes, Implantable pacing lead technology, IEEE Eng. Med. Biol. 9 (1990) 43–49.
[3] H. Matusiewicz, Potential release of in vivo trace metals from metallic medical implants in the human body: from ions to nanoparticles–a systematic analytical review, Acta Biomater. 10 (2014) 2379–2403.
[4] T. Hanawa, Metal ion release from metal implants, Mat. Sci. Eng. C-Mater. 24 (2004) 745–752.
[5] L. Perry, F. Karp, K. Hauch, B.D. Ratner, Explanted pacemakers: observations of the long-term foreign body response, Interface 4 (2007) 11.
[6] T. Weigel, T. Schmitz, T. Pfister, S. Gaetzner, M. Jannasch, R. Al-Hijailan, S. Schürlein, S. Suliman, K. Mustafa, J. Hansmann, A three-dimensional hybrid pacemaker electrode seamlessly integrates into engineered, functional human cardiac tissue in vitro, Sci. Rep. 8 (2018) 1–13.
[7] O. Veiseh, J.C. Doloff, M. Ma, A.J. Vegas, H.H. Tam, A.R. Bader, J. Li, E. Langan, J. Wyckoff, W.S. Loo, Size-and shape-dependent foreign body immune response to materials implanted in rodents and non-human primates, Nat. Mater. 14 (2015) 643–651.
[8] M.H. Schoenfisch, M. Ovadia, J.E. Pemberton, Covalent surface chemical modification of electrodes for cardiac pacing applications, J. Biomed. Mater. Res. 51 (2000) 209–215.
[9] H.G. Mond, J.R. Helland, K. Stokes, G.A. Bornzin, R. McVENES, The electrode-tissue interface: the revolutionary role of steroid-elution, Pacing Clin. Electrophysiol. 37 (2014) 1232–1249.
[10] C. Paech, M. Kostelka, I. Dähnert, P. Flosdorff, F.T. Riede, R.A. Gebauer, Performance of steroid eluting bipolar epicardial leads in pediatric and congenital heart disease patients: 15 years of single center experience, J. Cardiothorac. Surg. 9 (2014) 84.
[11] S.-M. Kim, N. Kim, Y. Kim, M.-S. Baik, M. Yoo, D. Kim, W.-J. Lee, D.-H. Kang, S. Kim, K. Lee, High-performance, polymer-based direct cellular interfaces for electrical stimulation and recording, NPG Asia Mater. 10 (2018) 255–265.
[12] J. Ren, Q. Xu, X. Chen, W. Li, K. Guo, Y. Zhao, Q. Wang, Z. Zhang, H. Peng, Y.G. Li, Superaligned carbon nanotubes guide oriented cell growth and promote electrophysiological homogeneity for synthetic cardiac tissues, Adv. Mater. 29 (2017), 1702713.
[13] Y. Zhu, K. Liu, J. Deng, J. Ye, F. Ai, H. Ouyang, T. Wu, J. Jia, X. Cheng, X. Wang, 3D printed zirconia ceramic hip joint with precise structure and broad-spectrum antibacterial properties, Int. J. Nanomed. 14 (2019) 5977.
[14] F. Bucciotti, M. Mazzocchi, A. Bellosi, Perspectives of the Si3N4-TiN ceramic composite as a biomaterial and manufacturing of complex-shaped implantable devices by electrical discharge machining (EDM), J. Appl. Biomater. Biomech. 8 (2010) 28–32.
[15] K. Shen, M.M. Maharbiz, Design of ceramic packages for ultrasonically coupled implantable medical devices, IEEE Trans. Biomed. Eng. 67 (2020) 2230–2240.
[16] L. Liu, R. Zhou, S. Yuan, Z. Sun, X. Lu, J. Li, F. Chu, A.D. Walmsley, B. Yan, L. Wang, Simulation training for ceramic crown preparation in the dental setting using a virtual educational system, Eur. J. Dent. Educ. 24 (2020) 199–206.
[17] S. Rahimi, F. SharifianJazi, A. Esmaeilkhanian, M. Moradi, A.H.S. Samghabadi, Effect of SiO2 content on Y-TZP/Al2O3 ceramic-nanocomposite properties as potential dental applications, Ceram. Int. 46 (2020) 10910–10916.
[18] L. Zhang, X. Liu, M. Li, E. Xu, F. Zhao, H. Yuan, X. Sun, C. Zhang, L. Gao, J. Gao, Feasibility of SiAlON–Si3N4 composite ceramic as a potential bone repairing material, Ceram. Int. 46 (2020) 1760–1765.
[19] X. Du, S. Fu, Y. Zhu, 3D printing of ceramic-based scaffolds for bone tissue engineering: an overview, J. Mater. Chem. B 6 (2018) 4397–4412.
[20] R.G. Ribas, V.M. Schatkoski, T.L. do Amaral Montanheiro, B.R.C. de Menezes, C. Stegemann, D.M.G. Leite, G.P. Thim, Current advances in bone tissue engineering concerning ceramic and bioglass scaffolds: a review, Ceram. Int. 45 (2019) 21051–21061.
[21] P. Colombo, G. Mera, R. Riedel, G.D. Soraru, Polymer-derived ceramics: 40 years of research and innovation in advanced ceramics, J. Am. Ceram. Soc. 93 (2010) 1805–1837.
[22] L.-A. Liew, W. Zhang, V.M. Bright, L. An, M.L. Dunn, R. Raj, Fabrication of SiCN ceramic MEMS using injectable polymer-precursor technique, Sensor. Actuator. A 89 (2001) 64–70.
[23] J. Grossenbacher, M.R. Gullo, R. Grandjean, T. Kiefer, J. Brugger, Sub micrometer ceramic structures fabricated by molding a polymer-derived ceramic, Microelectron. Eng. 97 (2012) 272–275.
[24] J. Grossenbacher, M.R. Gullo, V. Bakumov, G. Blugan, J. Kuebler, J. Brugger, On the micrometre precise mould filling of liquid polymer derived ceramic precursor for 300-μm-thick high aspect ratio ceramic MEMS, Ceram. Int. 41 (2015) 623–629.
[25] P.V.W. Sasikumar, G. Blugan, N. Casati, E. Kakkava, G. Panusa, D. Psaltis, J. Kuebler, Polymer derived silicon oxycarbide ceramic monoliths: microstructure development and associated materials properties, Ceram. Int. 44 (2018) 20961–20967.
[26] P. Jana, E. Zera, G.D. Sorarù, Processing of preceramic polymer to low density silicon carbide foam, Mater. Des. 116 (2017) 278–286.
[27] J. Grossenbacher, J. Brugger, R.M. Gullo, Development of Implantable Electrodes Based on Polymer Derived Ceramics, EPFL, 2015, https://doi.org/10.5075/epfl-thesis-5983.
[28] F. Dalcanale, Polymer Derived Ceramics Process in Biomedical Applications: Pacemaker Electrode, ETH Zurich, 2017, https://doi.org/10.3929/ethz-b-000245156.
[29] G. Perale, C. Giordano, F. Daniele, M. Masi, P. Colombo, L. Gottardo, S. Maccagnan, A novel process for the manufacture of ceramic microelectrodes for biomedical applications, Int. J. Appl. Ceram. Technol. 5 (2008) 37–43.
[30] M. Arango-Ospina, F. Xie, I. Gonzalo-Juan, R. Riedel, E. Ionescu, A.R. Boccaccini, Silicon oxycarbide based materials for biomedical applications, Appl. Mater. Today 18 (2020), 100482.
[31] C. Vakifahmetoglu, D. Zeydanli, P. Colombo, Porous polymer derived ceramics, Mater. Sci. Eng. R Rep. 106 (2016) 1–30.
[32] F. Dalcanale, J. Grossenbacher, G. Blugan, M.R. Gullo, A. Lauria, J. Brugger, H. Tevaearai, T. Graule, M. Niederberger, J. Kuebler, Influence of carbon enrichment on electrical conductivity and processing of polycarbosilane derived ceramic for MEMS applications, J. Eur. Ceram. Soc. 34 (2014) 3559–3570.
[33] F. Dalcanale, J. Grossenbacher, G. Blugan, M.R. Gullo, J. Brugger, H. Tevaearai, T. Graule, J. Kuebler, Cnt, PDCs, A fruitful association? Study of a polycarbosilane–MWCNT composite, J. Eur. Ceram. Soc. 35 (2015) 2215–2224.
[34] J. Grossenbacher, M.R. Gullo, F. Dalcanale, G. Blugan, J. Kuebler, S. Lecaudé, H. Tevaearai Stahel, J. Brugger, Cytotoxicity evaluation of polymer-derived ceramics for pacemaker electrode applications, J. Biomed. Mater. Res. A 103 (2015) 3625–3632.
[35] P. Vallachira Warriam Sasikumar, E. Mueller, P. Clement, J. Jang, E. Kakkava, G. Panusa, D. Psaltis, K. Maniura-Weber, M. Rottmar, J. Brugger, In vitro cytocompatibility assessment of Ti-modified silicon-oxycarbide based polymer-derived ceramic implantable electrodes under pacing conditions, ACS Appl. Mater. Interfaces 12 (2020) 17244–17253.
[36] D.R. Merrill, M. Bikson, J.G. Jefferys, Electrical stimulation of excitable tissue: design of efficacious and safe protocols, J. Neurosci. Methods 141 (2005) 171–198.
[37] S.F. Cogan, Neural stimulation and recording electrodes, Annu. Rev. Biomed. Eng. 10 (2008) 275–309.

[38] A. Norlin, Investigation of Electrochemical Properties and Performance of Stimulation/sensing Electrodes for Pacemaker Applications, KTH, 2005.
[39] A. Norlin, J. Pan, C. Leygraf, Investigation of electrochemical behavior of stimulation/sensing materials for pacemaker electrode applications I. Pt, Ti, and TiN coated electrodes, J. Electrochem. Soc. 152 (2005) J7–J15.
[40] A. Norlin, J. Pan, C. Leygraf, Investigation of electrochemical behavior of stimulation/sensing materials for pacemaker electrode applications II. Conducting oxide electrodes, J. Electrochem. Soc. 152 (2005) J85–J92.
[41] A. Norlin, J. Pan, C. Leygraf, Electrochemical behavior of Stimulation/ sensing materials for pacemaker electrode applications III. Nanoporous and smooth carbon electrodes, J. Electrochem. Soc. 152 (2005) J110–J116.
[42] J. Grossenbacher, M. Gullo, S. Lecaudé, H.T. Stahel, J. Brugger, SU-8 C-MEMS as candidate for long-term implantable pacemaker micro electrodes, in: 2015 Transducers-2015 18th International Conference on Solid-State Sensors, Actuators and Microsystems (TRANSDUCERS), IEEE, 2015, pp. 867–870.
[43] Y.J. Lee, H.-J. Kim, S.H. Do, J.Y. Kang, S.H. Lee, Characterization of nerve-cuff electrode interface for biocompatible and chronic stimulating application, Sens. Actuators, B 237 (2016) 924–934.
[44] N. Vachicouras, O. Tarabichi, V.V. Kanumuri, C.M. Tringides, J. Macron, F. Fallegger, Y. Thenaisie, L. Epprecht, S. McInturff, A.A. Qureshi, Microstructured thin-film electrode technology enables proof of concept of scalable, soft auditory brainstem implants, Sci. Transl. Med. 11 (2019), eaax9487.
[45] Y.N. Kang, N. Chou, J.-W. Jang, D. Byun, H. Kang, D.-J. Moon, J. Kim, S. Kim, An intrafascicular neural interface with enhanced interconnection for recording of peripheral nerve signals, IEEE Trans. Neural Syst. Rehabil. Eng. 27 (2019) 1312–1319.
[46] J. Jang, J.y. Kim, Y.C. Kim, S. Kim, N. Chou, S. Lee, Y.H. Choung, S. Kim, J. Brugger, H. Choi, A 3D microscaffold cochlear electrode array for steroid elution, Adv. Healthc. Mater. 8 (2019), 1900379.
[47] J. Jeong, S.H. Bae, J.-M. Seo, H. Chung, S.J. Kim, Long-term evaluation of a liquid crystal polymer (LCP)-based retinal prosthesis, J. Neural. Eng. 13 (2016), 025004.
[48] E. Hernández-Balaguera, E. López-Dolado, J. Polo, In vivo rat spinal cord and striated muscle monitoring using the current interruption method and bioimpedance measurements, J. Electrochem. Soc. 165 (2018) G3099.
[49] A.R. Harris, C. Newbold, R. Cowan, G.G. Wallace, Insights into the electron transfer kinetics, capacitance and resistance effects of implantable electrodes using fourier transform AC voltammetry on platinum, J. Electrochem. Soc. 166 (2019) G131.
[50] H. Hou, L. Li, Y. Cho, P. De Figueiredo, A. Han, Microfabricated microbial fuel cell arrays reveal electrochemically active microbes, PloS One 4 (2009).
[51] N. Zhang, F. Stauffer, B.R. Simona, F. Zhang, Z.-M. Zhang, N.-P. Huang, J. Vörös, Multifunctional 3D electrode platform for real-time in situ monitoring and stimulation of cardiac tissues, Biosens. Bioelectron. 112 (2018) 149–155.
[52] S. Nimbalkar, E. Castagnola, A. Balasubramani, A. Scarpellini, S. Samejima, A. Khorasani, A. Boissenin, S. Thongpang, C. Moritz, S. Kassegne, Ultra-capacitive carbon neural probe allows simultaneous long-term electrical stimulations and high-resolution neurotransmitter detection, Sci. Rep. 8 (2018) 1–14.
[53] A.S. Bandarenka, Exploring the interfaces between metal electrodes and aqueous electrolytes with electrochemical impedance spectroscopy, Analyst 138 (2013) 5540–5554.
[54] I.S. Kwon, Y.J. Kim, L. Klosterman, M. Forssell, G.K. Fedder, C.J. Bettinger, In vitro electrochemical characterization of polydopamine melanin as a tissue stimulating electrode material, J. Mater. Chem. B 4 (2016) 3031–3036.
[55] S. Meijs, M. McDonald, S. Sørensen, K. Rechendorff, L. Fekete, L. Klimša, V. Petrák, N. Rijkhoff, A. Taylor, M. Nesládek, Diamond/porous titanium nitride electrodes with superior electrochemical performance for neural interfacing, Front. Bioeng. Biotech. 6 (2018) 171.
[56] Q. Zeng, K. Xia, Y. Zhang, T. Wu, Well controlled 3D iridium oxide/platinum nanocomposites with greatly enhanced electrochemical performances, Adv. Mater. Interfaces 6 (2019), 1900356.
[57] J. Chen, X. Zheng, Y. Li, H. Zheng, Y. Liu, S.-i. Suye, A glucose biosensor based on direct electron transfer of glucose oxidase on PEDOT modified microelectrode, J. Electrochem. Soc. 167 (2020), 067502.
[58] I. Jeerapan, S. Poorahong, Flexible and stretchable electrochemical sensing systems: materials, energy sources, and integrations, J. Electrochem. Soc. 167 (2020), 037573.
[59] B.T. Seaton, D.F. Hill, S.L. Cowen, M.L. Heien, Mitigating the effects of electrode biofouling-induced impedance for improved long-term electrochemical measurements in vivo, Anal. Chem. 92 (2020) 6334–6340.
[60] B. Shafer, C. Welle, S. Vasudevan, A rat model for assessing the long-term safety and performance of peripheral nerve electrode arrays, J. Neurosci. Methods (2019), 108437.
[61] S. Meijs, K. Rechendorff, S. Sørensen, N.J. Rijkhoff, Corrosion study of implanted TiN electrodes using excessive electrical stimulation in minipigs, Metals 9 (2019) 389.
[62] I. Smokovych, M. Krüger, M. Scheffler, Polymer derived ceramic materials from Si, B and MoSiB filler-loaded perhydropolysilazane precursor for oxidation protection, J. Eur. Ceram. Soc. 39 (2019) 3634–3642.
[63] D.L. Poerschke, A. Braithwaite, D. Park, F. Lauten, Crystallization behavior of polymer-derived Si-OC for ceramic matrix composite processing, Acta Mater. 147 (2018) 329–341.
[64] E. Ionescu, S. Bernard, R. Lucas, P. Kroll, S. Ushakov, A. Navrotsky, R. Riedel, Polymer-derived ultra-high temperature ceramics (UHTCs) and related materials, Adv. Eng. Mater. 21 (2019), 1900269.
[65] R. Sujith, S. Jothi, A. Zimmermann, F. Aldinger, R. Kumar, Mechanical behaviour of polymer derived ceramics–a review, Int. Mater. Rev. (2020) 1–24.
[66] F. Maiullari, M. Costantini, M. Milan, V. Pace, M. Chirivì, S. Maiullari, A. Rainer, D. Baci, H.E.-S. Marei, D. Seliktar, A multi-cellular 3D bioprinting approach for vascularized heart tissue engineering based on HUVECs and iPSC-derived cardiomyocytes, Sci. Rep. 8 (2018) 1–15.
[67] I. Gonzalo-Juan, R. Detsch, S. Mathur, E. Ionescu, A.R. Boccaccini, R. Riedel, Synthesis and in vitro activity assessment of novel silicon oxycarbide-based bioactive glasses, Materials 9 (2016) 959.